A Bilateral Schema for Interval-Valued Image Differentiation

C. Lopez-Molina, C. Marco-Detchart,
L. De Miguel, H. Bustince, J. Fernandez
Dpto. Automatica y Computacion
Universidad Publica de Navarra
Pamplona, Spain
carlos.lopez@unavarra.es

B. De Baets
Kermit, Dept. of Math. Model., Statistics and Bioinformatics
Ghent University
Ghent, Belgium
bernard.debaets@ugent.be

***Abstract*—Differentiation of interval-valued functions is an intricate problem, since it cannot be defined as a direct generalization of differentiation of scalar ones. Literature on interval arithmetic contains proposals and definitions for differentiation, but their semantic is unclear for the cases in which intervals represent the ambiguity due to hesitancy or lack of knowledge. In this work we analyze the needs, tools and goals for interval-valued differentiation, focusing on the case of interval-valued images. This leads to the formulation of a differentiation schema inspired by bilateral filters, which allows for the accommodation of most of the methods for scalar image differentiation, but also takes support from interval-valued arithmetic. This schema can produce area-, segment- and vector-valued gradients, according to the needs of the image processing task it is applied to. Our developments are put to the test in the context of edge detection.**

1. Introduction

Due to technical and economic reasons, digital sampling has become the most common way to measure and store continuous facts, e.g. visual or acoustic information. The discretization processes faced by the original information necessarily lead to missing (or losing) a portion of it, simply because the range of possible measured values is limited to a predefined set. In the case of digital imagery, the loss of information inherent to the image model (e.g. the limitation in the number of tones) is combined with quality losses alien to it (e.g. lens noise or broken cells in a sensor). This fact holds for any possible coding or compression schema used in the representation of the digital image. Hence, automatic processing tools must deal with some uncerainty in the visual data.

Uncertainty in digital images is often considered in image processing literature, although its modelling is commonly implicit or simply missing. In some cases, e.g. when the uncertainty is believed to be due to noise, literature exposes explicit models, often in the shape of statistical distributions. There is also authors using fuzzy set theory to understand image data throughout the prism of hesitancy, e.g. modelling/training membership functions [1], [2], which allow automatic procedures to adapt to the conditions of each specific image. This can be seen as an implicit adaptation to the uncertainty of the initial data, even if that uncertainty is not explicitly enunciated. Also, some authors have simply developed robust tools and methods which overcome the potential problems due to uncertainty (as noise, contamination, heterogeneous or damaging lightning) not properly modelling it [3], [4].

In this work we do not intend to produce uncertainty models, or operators/procedures able to cope with it. Instead, we intend to convert original (scalar) images into a representation that includes, in an explicit manner, the uncertainty. In this way, we do not consider the uncertainty to be alien to the image model, but intrinsic to it. More specifically, we recall an interval-valued representation of images, aimed at capturing the inherent (and unavoidable) ambiguity in the imagery acquisition process. Then, we tackle the computation of partial derivatives on such representation of the imag. We focus on the construction of gradients (or gradient estimations), and present a bilateral schema [5] to compute the partial derivatives of an interval-valued image. In our proposal, such derivatives are represented by intervals, leading to an area-valued gradient. We analyze this representation of the gradient, and also study how to process it to express the gradient as the combination of an orientation and an interval-valued magnitude. The utility of the interval-valued images and our gradient extraction schema it tested in the context of edge detection. Specifically, we compare the performance of the bilateral differentiation schema in both scalar- and interval-valued image. The performance of such filters in both scalar and interval-valued images is studied on a well-known dataset.

The remainder of this work is organized as follows. In Section 2 we introduce the generation of interval-valued images by considering the measurement error in digital images, and we also recap some considerations on the differentiation of interval-valued image data. Then, in Section 3 we present a method to extract gradients from interval-valued images using a bilateral schema. Our developments are applied in Section 4 to edge detection, one of the most recurrent usages of gradients in image processing. A brief discussion is included in Section 5.

978-1-5090-0626-7/16/$31.00 ©2016 IEEE

2. Uncertainty in digital imagery

2.1. Image representation

In this work we consider images to be matrices of M rows and N columns, so that $\Omega = \{1, \ldots, M\} \times \{1, \ldots, N\}$ is the set of their positions. Given an image I, the value of a pixel at a certain position $\mathbf{p} \in \Omega$, is referred to as $I(\mathbf{p})$ (e.g. may an image I be grayscale, then $I(\mathbf{p}) \in \{0, \ldots, 255\}$). Moreover, we denote as $n(\mathbf{p}) \subset \Omega$ to the set of positions in a 3×3 neighbourhood centered at $\mathbf{p}$, including itself. Unless $\mathbf{p}$ belongs to the margin of the image, we have $|n(\mathbf{p})| = 9$.

2.2. Interval-valued images

Digital images, as any product of a discretization process, compel the analysis of their ambiguity and/or uncertainty. Common operations in image processing are, at least partially, imposed by this fact. Regularization (a.k.a. smoothing), for example, aims at producing a version of the image free from imperfections and artifacts not due to the visible scene. Fuzzy set theory, both in a narrow or wide sense [6], appears as a natural tool for the analysis of ambiguity in images. Operators and principles of fuzzy set theory are indeed used at almost any step of image analysis, from image interpretation [7], [8] to feature post-processing [2]. The techniques used for such proposals are diverse, and include, e.g., fuzzy inference systems [2], fuzzy morphology [9] and fuzzy peer groups [10]. The variety of techniques has naturally lead to the representation of images and visual features using Fuzzy Sets (FSs), but also generalizations as Interval-Valued Fuzzy Sets (IVFSs) [11] and Type-2 Fuzzy Sets (T2FSs) [12].

In [13] we propose an interval-valued representation of images, in an attempt to model the inherent ambiguity in the image acquisition process. Our idea roots on the fact that, although relevant exceptions hold, digital images are the result of a discretization of the real world. That is, images are discrete, sampled versions of continuous facts, e.g. lightning (conventional photography) or echoes to radio signals (SAR imagery). This discretization involves several sources of uncertainty or ambiguity. Most of them are contextual, in the sense that they could be present (or not) in an image, depending on the situation the image was acquired at (e.g. noise, distorting illumination or shading). Additionally, there is a source of uncertainty which is inherent to the very nature of digital images: the measurement error. The image acquisition process imposes the discretization in two aspects, spatial and tonal, each producing a measurement error:

- *Spatial error:* Surfaces and objects visible in an image are continuous in reality, and their boundaries can hardly coincide with those of the pixels in a pixel grid. In fact, often even humans disagree on which object does a pixel belong to. Due to the pixel grid model, the digital representation of a scene might be misplacing any object, or part of an object, by 1 position in any direction.
- *Tonal error:* Pixel values are taken from a finite number of tones. There are usually 2^8 tones in a grayscale image and 2^{24} in a RGB one, but, even using more bits per pixel, there is always a limit in the tonal precision. Hence, the measure error associated to the tone of the pixel is $\pm$ 1 tone.

Scalar images are not convenient to represent both errors (indeed, not even one of them). We propose in [13] an interval-valued representation of images, which accounts for spatial and tonal errors in an explicit manner. The construction is straightly driven from the above analysis of the measurement error. Let I be a grayscale image. The image I_{IV} generated from I is given by

$$I_{\text{IV}}(\mathbf{p}) = \Big[\max(0, \min_{\mathbf{q} \in n(\mathbf{p})} I(\mathbf{q}) - 1), \min(T_{\max}, \max_{\mathbf{q} \in n(\mathbf{p})} I(\mathbf{q}) + 1)\Big], \quad (1)$$

where $T_{\max}$ represents the maximum tonal value in the image representation. In Eq. (1) , each $\mathbf{p} \in \Omega$ is assigned an interval encompassing the brightness values in a 3×3 neighbourhood (assuming the spatial error), modified by $\pm$ 1 tone (because of the tonal error). The interpretation of this interval is dual. If considering that there exists one true value per pixel, then the interval embraces all of the possible values. Alternatively, if understanding that the actual value of a pixel cannot be scalar, and no single value can represent the information in that area of the scene, then the interval represents such range of tones. Images I_{IV}, generated as in Eq. (1), are referred to as Interval-Valued images (IV images).

Figure 1 displays the classical *House* image, together with the upper and lower bound of its interval-valued representation. Note that the upper and lower bounds of the IV image are similar to, e.g., dilated and eroded versions of the image [14], respectively. Analogously, the IV image is similar to that produced with upper-lower constructors, as presented in [11]. Other practical setups, or image acquisition processes, can also lead to images in which the tonal representation at each pixel is accommodated as an interval. High Dynamic Range (HDR) procedures [15], [16], as well as some multi-sensor satellital imagery (see, e.g. [17]) are based on the fusion of multiple tonal representations at each pixel, which could naturally lead to an interval-valued representation. Nevertheless, the semantics of the interval-valued information in such cases are completely different.

The construction of IV images is robust against some types of noise (as Gaussian one), but also quite sensitive to some other kinds of contamination (as impulsive or salt-and-pepper). Still, dealing with external sources of contamination is not the main goal of IV images, since they only intend to capture factors inherent to the image model. Interval-valued images provide, in our opinion, a truthful interpretation of the original images, since they use no information other than that in the scalar image. Hence, there is a need to develop basic processing tools and techniques to make them eligible for well-known image processing tasks.

(a) Original Image (b) IV image

Figure 1. The *House* image and the lower and upper bounds of its interval-valued representation, constructed as in Eq. (1).

2.3. Image differentiation

Differentiation is one of the most common operations in signal processing, in general, and image processing, in particular. However, images are meant to be discrete, in both spatial and tonal range. As a consequence, from a theoretical point of view, image differentiation is not possible or more precisely, it *is ill-posed in the sense of Hadamard* [18]. How to deal with this ill-posedness has been a recurrent area of research in past years, often leading to regularization schemes which minimized the effect of signal discretization [19], [20]. Note that regularization implies a certain loss of information, but when it comes to image processing, *discrete differences intended to approximate the derivatives yield "worse" results when refining the grid* [21].

Differentiation schemes for image processing attempt to compute the derivatives of the underlying signal, and hence, in a sense, focus on solving the problems due to discretization [22]. Several studies on the topic have been presented and, at least from a practical point of view, widely accepted [23], [24]. Generally, they involve both a regularization schema to avoid spurious artifacts in the original signal and a differentiation filter (kernel) to compute local differences. Regularization is typically based on Gaussian filters, since they are the only ones not producing new minima or maxima in the first derivative of a signal [20], while differentiation is often based on antisymmetric filters [25].

Image differences, as representatives of the underlying signal derivatives, are used in a range of tasks and applications. For example, to characterize a range of visual features, including image primitives (as Marr's primal sketch [22], [26]), low level features (as textures or boundaries) and large scale-structures (as ridges in fingertip prints). Also, they serve as support information for mid- or high-level tasks as segmentation, object tracking or image inpainting. All of such tasks are grounded on the analysis of the local variations of the image. Very interestingly, the non-homogeneous interpretation of local variations has subsequently rendered into variable representations. Even if restricting to first order differentiation, we find a range of representations in image processing literature. For example, active contours (a.k.a. snakes [27], [28]) are evolved and fitted using gradients, which capture the orientation and strength of the locally-maximal image variations. Diffusion processes were introduced with very simple differentiation models (as the 4-point model by Perona and Malik [29]), but quickly evolved to make use of tensors. Many diffusion-based processes (as image reconstruction [30], [31]) require tensorial descriptors in order to consider the anisotropy of local variation. The extraction of semi-local features, like texture, can be exclusively based on gradient direction analysis [32], making it unnecessary to compute the strength of the image variation. Interestingly, image differentiation, as a mean to study image variation, is widely accepted but has rendered in a variety of mathematical formulations.

There exists three main different embodiments of the idea of first order differences in an image, according to how they represent such differences:

- *Total variation.-* It is a scalar-valued measurement of the amount of tonal change at each pixel of the image[1]. The total variation does not hold information on the direction or directions in which image changes, what greatly eases its computation. Examples of procedures to compute total variation include SUSAN areas [34] or mathematical morphology-based operators [35].
- *Gradient.-* Gradient maps are the most common representation of image variation, but fall short in providing necessary information for certain tasks. Specifically, they hold no information on the variation orthonormal to that of the gradient itself. The popularity of the gradients is due, in a large portion, to the fact that most of the gradient characterization filters in the literature were designed for 1D signals, and relied on the straight projection of such signals in the secondary dimension [36], [37]. This simplification made it unnecessary to study the anisotropy of the signal, *i.e.* the variation of the image in the orthonormal direction.
- *Tensor.-* It is usually constructed from the first order partial derivatives in two orthogonal directions. Whichever directions are chosen, eigenvector analysis can lead to the characterization of the image variation in two or more directions. Although tensors are a less popular representation than gradients, they allow for the interpretation (and measurement) of the anisotropy of image variations, and hence have had great relevance for diffusion-based processes.

Each of these three representations of image differences is obtained by specialized means, but they usually involve some kind of local contrast measurement (for total variation), or convolution of the image with antisymmetric [25], and often steerable [38], filters (for gradients and tensors).

The differentiation problem for standard (scalar) images is well-studied, and its solutions have been ported to other types of images. For example, to multichannel images, in which pixels take up vectorial information. In such cases, the gradient at each pixel becomes a Jacobian matrix [39], [40], hampering its geometrical interpretation [41]. Our interest, however, lies on IV images.

1. Total variation is completely different from the notion of the Laplacian of the image (∇^2), which has also been used extensively for image analysis [22], [33].

3. Gradients on interval-valued images

In this section we study the characterization of gradients on IV images. The reason for restricting to gradients, avoiding total variation and tensors is twofold: first, the limited space; second, the fact that total variation measurements can be extracted from the gradients, e.g. from their magnitude, while tensors are indeed constructed by combining several oriented differences.

The gradient of a signal can be seen as the n-dimensional extension of the concept of derivative. It is mathematically modelled as the vector containing the first order partial derivative in n orthogonal directions. In this sense, being $S : \mathbb{R}^n \to \mathbb{R}$ any signal, its gradient at some position $\mathbf{i} = (i_1, \ldots, i_n) \in \mathbb{R}^n$ is given by

$$\nabla S(\mathbf{i}) = \left(\frac{\partial S(\mathbf{i})}{\partial x_1}, \ldots, \frac{\partial S(\mathbf{i})}{\partial x_n} \right) ,$$

with $(x_1, \ldots, x_n)$ representing a base of vectors in $\mathbb{R}^n$. Since image are discrete, the derivatives composing the gradient are approximated by discrete differentiation. Although several different strategies are applicable, most of the authors use specialized convolution filters for the task. The study of such operators is vast and detailed [23], [42].

To the best of our knowledge, no study has been performed on the differentiation of discrete interval-valued signals representing uncertainty. Some works have dealt with interval-valued differentiation (under different conditions), significant examples being those by Moore [43], Moore *et al.* [44] and Schöder [45] on interval-functions, or more recently, Lupulescu [46]. A review on interval analysis, which also covers differentiation, was presented by Alefeld and Mayer [47]. However, when it comes to discrete signals, it is also possible to extend well-known techniques on scalar-valued images to the interval-valued setup, as recap in this section.

A straightforward strategy for IV image differentiation consists of applying (scalar) differentiation on the upper and lower bounds of the intervals individually, as such bounds can be seen themselves scalar-valued images[2] (see Fig. 1). In our opinion, this strategy stems from considering each bound of the interval as independent information, what collides, at least partially, with the main idea behind IV images. Hence, we propose to evolve classical differentiation methods to allow for the introduction of interval-valued operators.

For the sake of compactness, we denote the vertical and horizontal partial differences $I_h(x,y) = \frac{\partial I(x,y)}{\partial x}$ and $I_v(x,y) = \frac{\partial I(x,y)}{\partial y}$, respectively. If opting by computing differences with filters, then $I_h = I * D_h$ and $I_v = I * D_v$, where D_h and D_v are convolution filters designed for differentiation. Note that, in most cases, D_h and D_v are rotations of each other.

2. Note that the gradient maps at each of the bounds do not necessarily cast the bounds of the interval valued map.

For a given $\mathbf{p} = (x,y)$, $\mathbf{p} \in \Omega$, we have[3]

$$I_h(\mathbf{p}) = \int_{i=-\infty}^{\infty} \int_{j=-\infty}^{\infty} I(\mathbf{p} + (i,j)) \cdot D_h(i,j) \, , \qquad (2)$$

what becomes, in a discrete universe,

$$I_h(\mathbf{p}) = \sum_{i=-\infty}^{\infty} \sum_{j=-\infty}^{\infty} I(\mathbf{p} + (i,j)) \cdot D_h(i,j) \, . \qquad (3)$$

Let D_h be antisymmetric w.r.t to the vertical axis, *i.e.* let $D_h(i,j) = -D_h(-i,j)$ for any $(i,j) \in \mathbb{R}^2$. Following the rationale in [25], we can rewrite (3) as:

$$I_h(\mathbf{p}) = \sum_{i=0}^{\infty} \sum_{j=-\infty}^{\infty} (I(\mathbf{p}+(i,j)) - I(\mathbf{p}+(-i,j))) \cdot D_h(i,j) \, . \quad (4)$$

Interestingly, we can reformulate $I_h(\mathbf{p})$ following the ideas behind bilateral filters [5]:

$$I_h(\mathbf{p}) = \sum_{i=0}^{k} \sum_{j=-k}^{k} d(I(\mathbf{p} + (i,j)), I(\mathbf{p} + (-i,j))) \cdot w(i,j) \, , \quad (5)$$

where d is a measure of dissimilarity between pixel tones and w quantifies the influence of a pixel displaced (i,j).

In order to compute a gradient from any two orthogonal derivatives, e.g. I_h and I_v, filters D_* need to be steerable. Otherwise, the filtering process has to consider any possible orientation in $[0, 2\pi[$, retaining the response with greatest magnitude [38].

The derivative of a signal I in direction $\theta \in [0, 2\pi[$ at $\mathbf{p} \in \Omega$, using the formulation in Eq. (5), is approximated as

$$I_\theta(\mathbf{p}) = \sum_{\mathbf{q} \in R_\theta} d(I(\mathbf{p} + \mathbf{q}), I(\mathbf{p} + m(\mathbf{q}, \theta))) \cdot w_\theta(\mathbf{q}) \, , \qquad (6)$$

where $R_\theta = \{\mathbf{v} \in \mathbb{Z}^2 \mid \mathbf{v} \cdot \mathbf{i}_\theta > 0\}$, with $\mathbf{i}_\theta$ the unit vector in the orientation θ, is the *positive* region of $\mathbb{Z}^2$ in such direction; $m(\mathbf{v}, \rho)$ is the mirroring of position of $\mathbf{v}$ w.r.t. the axis perpendicular to ρ; and w_θ is the rotation of the weighing function w according to θ.

Since the notion of steerability, as well as that of convolution, are lost in Eq. (5), the gradient of the image I at $\mathbf{p}$ is that in the direction $\varphi = \operatorname{argmax}_\theta I_\theta(p)$. The values I_h and I_v can be thereafter obtained by trigonometry.

Bilateral filtering for first order differentiation, as in Eq. (6) can be applied to IV images. Firstly, sums and scalar-to-interval products are defined in interval arithmetic [44]. Secondly, the function w_θ is oblivious of the value hold by each pixel, and so can be identical for scalar- or interval-valued images. Alternatives for w_θ include the positive part of well-known differentiation filters, but also inverted distance functions, zero-centered probability distribution functions (e.g. the Gaussian function), or any other function tending to zero[4]. Thirdly, regarding the function d, it can be easily ported from a scalar-valued ($(\mathbb{R})^2 \to \mathbb{R}$) to an IV setup ($(L([0,1]))^2 \to L([0,1])$), options ranging from interval arithmetic to comparison operators (as IV REFs [48]).

3. The computation of I_v is analogous, and hence omitted.

4. The weighing function w_θ, as any convolution filter, needs to tend to zero, otherwise the result is always infinite.

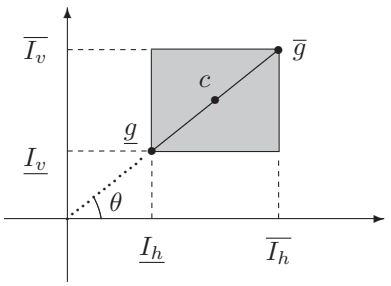

Figure 2. Visual representation of the area gradient and its conversion to a segment. The area is arbitrarily assumed to be in the first quadrant, but the intepretation analogous in any other quadrant.

The formulation Eq. (6) is, hence, a convenient approach to tackle differentiation on IV images. However, two questions related to the differentiation schema remain open. First, how to identify the *maximum* gradient or, more precisely, the direction in which the difference is maximum. Second, once that direction is computed, how to interpret the IV components of the gradient. Both are solved by computing the center of gravity of each oriented difference.

Figure 2 displays a schematic representation of the interpretation of $I_\theta(\mathbf{p})$ in IV images. Firstly, the center of gravity c for each orientation θ, *i.e.* c_θ, is given by the K_α operator, specifically by $K_{0.5}(I_\theta(\mathbf{p}))$. Note that the angle θ maximizing $||c_\theta||$, with $||\cdot||$ the Euclidean norm, is kept as gradient orientation. Secondly, the gradient of an IV image is not a vector in $\mathbb{R}^2$, but an area instead. This area can be seen as a projection of the uncertainty about the intensity of the pixels in the image. Since the initial data is unreliable, the uncertainty is propagated when measuring local features (in this case, the gradient). In case the center of gravity is the origin, the gradient has area zero. Also, if the area takes more than one quadrant, we only consider the area corresponding to the quadrant in which c is.

In order to ease the geometrical interpretation of the gradient of an IV image, we convert the area gradient into a segment gradient. That segment can be dually defined as (a) the segment with orientation θ and whose limit points are defined by their distance to the origin (the interval-valued magnitude) or as (b) the intersection of the gradient area and the line passing by the origin and intersecting the horizontal axis with angle θ. Note that the magnitude itself can be seen as an IVFS representation of the image total variation.

To sum up, the gradient at each position $\mathbf{p} \in \Omega$ of an IV image I is expressed as a segment determined by the angle

$$\varphi = \text{argmax}_{\theta \in [0,\pi[} \; K_{0.5}\left(I_\theta(\mathbf{p})\right) \, ,$$

and the IV magnitude obtained by $I_\varphi(\mathbf{p})$ (as in Eq. (6)) after performing the elementary interpretation of the negative values (negative values in $I_\varphi(\mathbf{p})$ stand for decrease in direction φ or equivalently, increase in direction $\varphi + \pi$). The segment-valued gradient can be turned into a vectorial gradient by aplying the K_α operator to its magnitude.

4. Experimental results

One of the most direct applications of gradient extraction is edge detection. The reason stems from two facts. First, the magnitude of the gradients can be used as cue for the discrimination of edge and non-edge pixels[5]. Second, the orientation of gradients can be used to perform 2D non-maxima suppression [50], in order to thin the edge segments.

The aim of this experiment is to check the effect of using IV images for edge detection. This section presents a comparison of two edge detection methods applicable to both scalar and IV images. The difference between them is the spatial term w_θ used in Eq. (6). The first method uses the zero-th order Gaussian kernel, while the second one uses the zero-th order Infinite Symmetric Exponential (ISE) kernel (it is, hence, computationally equivalent to the first order Shen-Castan filter [37]).

4.1. Algorithmic details

The edge detection procedure used in this experiment, according to the Bezdek Breakdown Structure [51], is as follows: Gaussian regularization for *conditioning*, gradient extraction as in Section 3, thinning using non-maxima suppression on the gradient map for *blending* and hysteresis for *scaling*. The thresholds for hysteresis are set using the double bowstring technique [52], which in standard conditions of the histogram, is the result of two consecutive applications of the Rosin method [53].

The procedure has two different parameters: the standard deviation used in the Gaussian filter for regularization that used in the functions for the spatial term. We refer to the former as σ_1, while the latter is σ_2 (for first order Gaussian kernels) or p (for the exponent of ISE kernel). Note that σ_2 and p are both used to control the size of the differentiation filter. However, their interpretation is opposed: while greater σ_2 leads to (spatially) larger convolution filters, greater p leads to smaller (equivalently, higher-frequency) filters. In this experiment we set $\sigma_1 = 2$, while the size-controlling parameters take values $\sigma_2 \in \{2, 3, 4\}$ and $p \in \{0.25, 0.5, 1\}$.

In order to threshold and binarize the gradients of IV images, the IV gradient needs to be converted to a regular (vectorial) gradient. This is done by keeping the orientation of the gradient, and using the K_α operator, with variable α, to convert the IV magnitude to a scalar magnitude.

The code for this experiment can be freely accessed as part of the Kermit Image Toolkit (KITT) [54].

4.2. Quantification of the results

The evaluation of edge detection results is an open debate [55]. For this work we take edge detection as a binary classification problem, which can be evaluated in terms of success and fallout. We compare the output by

5. Some authors have elaborated on non-linear mappings to model edge cues from gradient magnitudes [3], [49], but gradient magnitudes are often used, with no further processing, as single cue for edge discrimination.

an edge detection method with the human-made ground truth (GT) [56]. Each pixel in the candidate edge image is classified as true positive (TP), true negative (TN), false positive (FP) or false negative (FN).

The classification of each edge pixel, given a GT image, needs to consider a certain tolerance in the position of the same edge in two different images. An edge displaced from its true position should not be penalized as much as if it was completely missing. In order to solve this problem, we use a one-to-one pixel validation algorithm to validate the edge pixels in the candidate edge image w.r.t. those the GT one. This matching allows some spatial tolerance (in our case, up to 5 pixels, approx. 1% of the image diagonal); hence, an edge pixel slightly displaced from its true position can be validated, and consequently taken as a TP. The pixel-to-pixel matching is carried out using the validation technique by Estrada and Jepson [57]. This validation can be expressed as a mapping $\psi : \Omega \times \Omega \to \Omega$ so that $\psi(A, B) \subseteq A$ is the subset of boundary pixels in A that are validated w.r.t. B. From ψ, precision and recall are computed as

$$\textsc{Prec} = \frac{|\psi(E_{\text{cd}}, E_{\text{gt}})|}{|E_{\text{cd}}|} \quad \text{and} \quad \textsc{Rec} = \frac{|\psi(E_{\text{gt}}, E_{\text{cd}})|}{|E_{\text{gt}}|} \,.$$

where E_{cd} and E_{gt} are the candidate and GT images, respectively. An overall quality measurement of the a candidate boundary image is given by the well-known $\mathrm{F}_{\alpha=0.5}$ measure, *i.e.* the harmonic mean of PREC and REC.

In this experiment we have used the *test* subset of the Berkeley Segmentation Dataset (BSDS500) [58], containing 200 images, together with several hand-labelled GT images. For each GT image we keep the triplet for which $\mathrm{F}_{0.5}$ is maximal. That is, we compare the candidate image with each of its GT images. Then, the triplet (PREC,REC,$\mathrm{F}_{0.5}$) having the greatest $\mathrm{F}_{0.5}$ is considered as the evaluation of the detector for that candidate image.

4.3. Results

The results measured in the experiments are included in Fig. 3. Note that each method, when applied to IV images, is displayed as a plot, since they depend on the α value used to convert the segment gradient into a vector in $\mathbb{R}^2$. Then, the performance of the methods, when applied to scalar-valued images, is represented as a dot. This is done in order to avoid an excess of visual information. In any case, the background lines in the plots allow for easy scalar to interval-valued comparison.

The first observation is that both methods, obtain similar results, despite the use of rather different functions w_θ. This observation does not only hold in a general basis, but also in detailed pairwise comparisons. For example, similarities can be found between the performance reached by Gaussian kernels with the smallest σ_2 and those by exponential kernels with the greatest p (both plotted in red).

Another fact to be noticed in Fig. 3 is that the performance of the procedure is, regardless of its configuration, rather stable. Regarding PREC and REC, the differences are clear, with (spatially) larger filters obtaining greater precision and lower recall. This is concordant with studies in the literature [59], and is due to the avoidance of noise and texture, which comes coupled to missing some high-frequency edges. A related observation stems from the comparison of the PREC and REC values when using scalar or IV images. Interestingly, using IV images induces an increase of the precision, as well as a decrease of the recall. This is surprising, since the use of IV images increase the amount of information taken into account in the gradient computation at each position, what seems to be conceptually similar to enlarging the filters themselves. However, the induced effect is the opposite.

Regarding the $\mathrm{F}_{0.5}$ measure, the tested methods have relatively similar performances, all of them in $[0.45, 0.53]$. This leads to a twofold interpretation. On the one hand, the use of IV images does not have a significant impact in the results of the proposed edge detection methods. From this point of view, IV differentiation can be seen as pointless, or at least its usability can be said to be unproven. However, on the other hand we have that our procedure is able to handle a truthful version of the images (because of being discrete measurements, images *should* be interval-valued), with no loss of performance. This might indicate that we are prepared to take the IV images as starting basis for further developments. In our opinion, both interpretations are backed up by the results in Fig. 3. Nevertheless, it is worth noting that (a) the representativity of the present experiment is limited to the scope of edge detection, while gradients can be applied to many other tasks; also, that (b) there is a number of external factors, mostly due to the other procedures in the edge detection process, which could have a certain impact in the results, and might distort the analysis.

5. Conclusions

We have analyzed the role of the measurement error in digital images, proposing an interval-valued representation of the image to overcome it. We understand that the IV images, as constructed in this work, are a truthful representation of the actual information in a scalar image. Moreover, with this representation, we model the measurement error which, due to the nature of digital imagery, is embedded in the initial data. We have also analyzed the challenges IV images pose for differentiation, which, despite ill-posed, is ubiquitous in image processing. In this work we propose a bilateral schema for first order IV image differentiation. This schema has produced two edge detection methods for IV images, based on Gaussian and infinite symmetric exponential spatial kernels, respectively. Our experimental setup analyzes the differences in the performance of these methods on scalar (standard) and IV images. From the results in this experiment we can infer that the performance of the edge detection methods do not vary significantly when using IV images. However, we consider that our construction offers new opportunities to design tailor-made operators for IV images, which might fully exploit its enhanced representation of hesitancy.

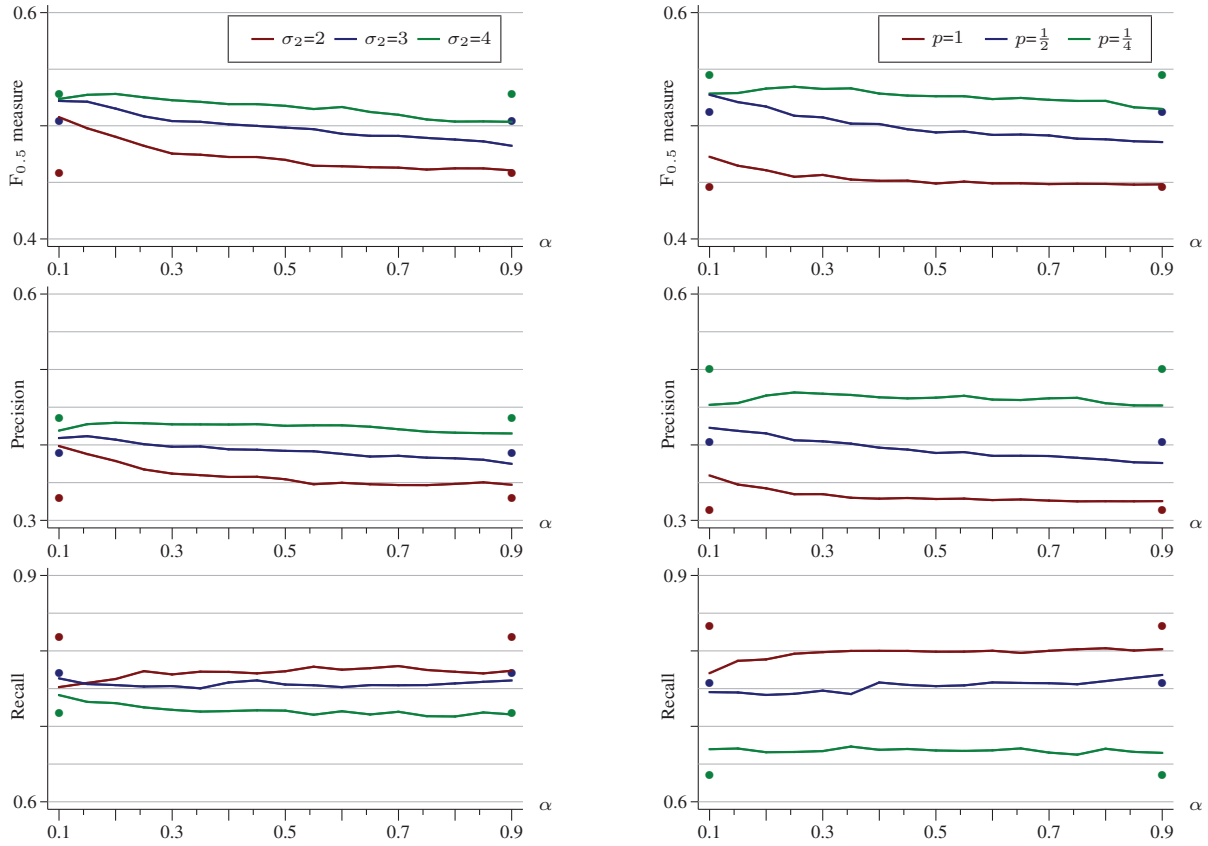

(a) Gaussian spatial term

(b) Inverted Exponential spatial term

Figure 3. Results on the proposed edge detection procedure using two different families of spatial term functions, applied on both IV and scalar-valued images. Each line corresponds to a different parameterization on IV images, while dots represent the performances on scalar-valued images. Note that the dots corresponding to the results on scalar-valued images are duplicated to ease the visual analysis.

Acknowledgements

The authors gratefully acknowledge the financial support received from the Spanish Ministry of Science (project TIN2013-40765-P), the Research Services of the Universidad Publica de Navarra and the Research Foundation Flanders (FWO project 3G.0838.12.N).

References

[1] F. Russo, "FIRE operators for image processing," *Fuzzy Sets and Systems*, vol. 103, no. 2, pp. 265–275, 1999.

[2] T. Law, H. Itoh, and H. Seki, "Image filtering, edge detection, and edge tracing using fuzzy reasoning," *IEEE Trans. on Pattern Analysis and Machine Intelligence*, vol. 18, no. 5, pp. 481–491, 1996.

[3] M. Black, G. Sapiro, D. Marimont, and D. Heeger, "Robust anisotropic diffusion," *IEEE Trans. on Image Processing*, vol. 7, no. 3, pp. 421–432, 1998.

[4] E. Nezhadarya and R. K. Ward, "A new scheme for robust gradient vector estimation in color images," *IEEE Trans. on Image Processing*, vol. 20, no. 8, pp. 2211–2220, 2011.

[5] C. Tomasi and R. Manduchi, "Bilateral filtering for gray and color images," in *Proc. of the IEEE International Conf. on Computer Vision*, 1998, pp. 838–846.

[6] L. A. Zadeh, "Soft computing and fuzzy logic," *IEEE Software*, vol. 11, no. 6, pp. 48–56, 1994.

[7] F. Jacquey, F. Comby, and O. Strauss, "Fuzzy edge detection for omnidirectional images," *Fuzzy Sets and Systems*, vol. 159, no. 15, pp. 1991–2010, 2008.

[8] S. K. Pal and R. A. King, "On edge detection of X-Ray images using fuzzy sets," *IEEE Trans. on Pattern Analysis and Machine Intelligence*, vol. 5, no. 1, pp. 69–77, 1983.

[9] J.-A. Jiang, C.-L. Chuang, Y.-L. Lu, and C.-S. Fahn, "Mathematical-morphology-based edge detectors for detection of thin edges in low-contrast regions," *IET Image Processing*, vol. 1, no. 3, pp. 269–277, 2007.

[10] S. Morillas, V. Gregori, and A. Hervas, "Fuzzy peer groups for reducing mixed Gaussian-impulse noise from color images," *IEEE Trans. on Image Processing*, vol. 18, no. 7, pp. 1452–1466, 2009.

[11] E. Barrenechea, H. Bustince, B. De Baets, and C. Lopez-Molina, "Construction of interval-valued fuzzy relations with application to the generation of fuzzy edge images," *IEEE Trans. on Fuzzy Systems*, vol. 19, no. 5, pp. 819–830, 2011.

[12] P. Melin, C. I. Gonzalez, J. R. Castro, O. Mendoza, and O. Castillo, "Edge-detection method for image processing based on generalized type-2 fuzzy logic," *IEE Trans. on Fuzzy Systems*, vol. 22, no. 6, pp. 1515–1525, 2014.

[13] C. Lopez-Molina, C. Marco-Detchart, J. Cerron, H. Bustince, and B. De Baets, "Gradient extraction operators for discrete interval-valued data," in *Proc. of the Conf. of the International Fuzzy Set Association*, 2015.

[14] J. Serra, "Introduction to mathematical morphology," *Computer Vision, Graphics, and Image Processing*, vol. 35, no. 3, pp. 283–305, 1986.

[15] P. E. Debevec and J. Malik, "Recovering high dynamic range radiance maps from photographs," in *ACM SigGraph 2008*. ACM, 2008, p. 31.

[16] E. Reinhard, W. Heidrich, P. Debevec, S. Pattanaik, G. Ward, and K. Myszkowski, *High dynamic range imaging: acquisition, display, and image-based lighting*. Morgan Kaufmann, 2010.

[17] L. Wald, T. Ranchin, and M. Mangolini, "Fusion of satellite images of different spatial resolutions: assessing the quality of resulting images," *Photogrammetric engineering and remote sensing*, vol. 63, no. 6, pp. 691–699, 1997.

[18] V. Torre and T. Poggio, "On edge detection," *IEEE Trans. on Pattern Analysis and Machine Intelligence*, vol. 8, no. 2, pp. 147–163, 1984.

[19] A. P. Witkin, "Scale-space filtering," in *Proc. of the International Joint Conf. on Artificial Intelligence*, vol. 2, 1983, pp. 1019–1022.

[20] J. Babaud, A. P. Witkin, M. Baudin, and R. O. Duda, "Uniqueness of the Gaussian kernel for scale-space filtering," *IEEE Trans. on Pattern Analysis and Machine Intelligence*, vol. 8, no. 1, pp. 26–33, 1986.

[21] L. Florack, *Image structure*. Springer Science & Business Media, 1997, vol. 10.

[22] D. Marr and E. Hildreth, "Theory of edge detection," *Proceedings of the Royal Society of London*, vol. 207, no. 1167, pp. 187–217, 1980.

[23] J. M. S. Prewitt, *Object enhancement and extraction*, ser. Picture Processing and Psychopictorics. Academic Press, 1970, pp. 75–149.

[24] V. Torre and T. Poggio, "Differential operators for edge detection," Massachusetts Institute of Technology, Tech. Rep., 1983.

[25] N. Madrid, C. Lopez-Molina, and B. De Baets, "Generalized anti-symmetric fiters for edge detection," in *Proc. of the Conf. of Soft Computing and Pattern Recognition*, 2013.

[26] D. Marr, *Vision*. MIT Press, 1982.

[27] M. Kass, A. P. Witkin, and D. Terzopoulos, "Snakes: Active contour models," *International Journal of Computer Vision*, vol. 4, pp. 321–331, 1988.

[28] V. Caselles, F. Catté, T. Coll, and F. Dibos, "A geometric model for active contours in image processing," *Numerische Mathematik*, vol. 66, pp. 1–31, 1993.

[29] P. Perona and J. Malik, "Scale-space and edge detection using anisotropic diffusion," *IEEE Trans. on Pattern Analysis and Machine Intelligence*, vol. 12, no. 7, pp. 629–639, 1990.

[30] I. Galić, J. Weickert, M. Welk, A. Bruhn, A. Belyaev, and H.-P. Seidel, "Image compression with anisotropic diffusion," *Journal of Mathematical Imaging and Vision*, vol. 31, pp. 255–269, 2008.

[31] M. Mainberger, A. Bruhn, J. Weickert, and S. Forchhammer, "Edge-based compression of cartoon-like images with homogeneous diffusion," *Pattern Recognition*, vol. 44, no. 9, pp. 1859–1873, 2011.

[32] A. Rao and B. Schunck, "Computing oriented texture fields," in *IEEE Conf. on Computer Vision and Pattern Recognition*, 1989, pp. 61–68.

[33] W. E. L. Grimson and E. C. Hildreth, "Comments on "Digital step edges from zero crossings of second directional derivatives"," *IEEE Trans. on Pattern Analysis and Machine Intelligence*, vol. 7, no. 1, pp. 121–127, 1985.

[34] S. M. Smith and J. M. Brady, "SUSAN- a new approach to low level image processing," *International Journal of Computer Vision*, vol. 23, pp. 45–78, 1997.

[35] J. Lee, R. Haralick, and L. Shapiro, "Morphologic edge detection," *IEEE Journal of Robotics and Automation*, vol. 3, no. 2, pp. 142–156, 1987.

[36] J. Canny, "A computational approach to edge detection," *IEEE Trans. on Pattern Analysis and Machine Intelligence*, vol. 8, no. 6, pp. 679–698, 1986.

[37] J. Shen and S. Castan, "An optimal linear operator for step edge detection," *CVGIP: Graphical Models and Image Processing*, vol. 54, no. 2, pp. 112–133, 1992.

[38] W. Freeman and E. Adelson, "The design and use of steerable filters," *IEEE Trans. on Pattern Analysis and Machine Intelligence*, vol. 13, no. 9, pp. 891–906, 1991.

[39] J. Weickert, *Anisotropic Diffusion in Image Processing*, ser. ECMI Series. Teubner-Verlag, 1998.

[40] G. Sapiro, "Color snakes," Hewlett-Packard, Tech. Rep., 1995.

[41] S. Di Zenzo, "A note on the gradient of a multi-image," *Computer Vision, Graphics, and Image Processing*, vol. 33, no. 1, pp. 116–125, 1986.

[42] G. Papari and N. Petkov, "Edge and line oriented contour detection: State of the art," *Image and Vision Computing*, vol. 29, no. 2-3, pp. 79–103, 2011.

[43] R. Moore, *Interval Analysis*. Prentince-Hall, 1996.

[44] R. E. Moore, R. B. Kearfott, and M. J. Cloud, *Introduction to interval analysis*. Society for Industrial and Applied Mathematics (SIAM), 2009.

[45] G. Schröder, "Differentiation of interval functions," *Proceedings of the American Mathematical Society*, vol. 36, no. 2, pp. 485–490, 1972.

[46] V. Lupulescu, "Fractional calculus for interval-valued functions," *Fuzzy Sets and Systems*, vol. 265, pp. 63–85, 2015.

[47] G. Alefeld and G. Mayer, "Interval analysis: theory and applications," *Journal of Computational and Applied Mathematics*, vol. 121, no. 1, pp. 421–464, 2000.

[48] A. Jurio, M. Pagola, D. Paternain, C. Lopez-Molina, and P. Melo-Pinto, "Interval-valued restricted equivalence functions applied on clustering techniques," in *Proc. of the IFSA-EUSFLAT*, 2009, pp. 831–836.

[49] C. Lopez-Molina, B. De Baets, and H. Bustince, "Generating fuzzy edge images from gradient magnitudes," *Computer Vision and Image Understanding*, vol. 115, no. 11, pp. 1571–1580, 2011.

[50] A. Rosenfeld and M. Thurston, "Edge and curve detection for visual scene analysis," *IEEE Trans. on Computers*, vol. 20, no. 5, pp. 562–569, 1971.

[51] J. Bezdek, R. Chandrasekhar, and Y. Attikouzel, "A geometric approach to edge detection," *IEEE Trans. on Fuzzy Systems*, vol. 6, no. 1, pp. 52–75, 1998.

[52] X. Liu, Y. Yu, B. Liu, and Z. Li, "Bowstring-based dual-threshold computation method for adaptive Canny edge detector," in *Proc. of the International Conf. of Image and Vision Computing New Zealand*, 2013, pp. 13–18.

[53] P. L. Rosin, "Unimodal thresholding," *Pattern Recognition*, vol. 34, no. 11, pp. 2083–2096, 2001.

[54] Kermit Research Unit (Ghent University), "The Kermit Image Toolkit (KITT)." [Online]. Available: www.kermitimagetoolkit.com

[55] C. Lopez-Molina, H. Bustince, and B. De Baets, "Separability criteria for the evaluation of boundary detection benchmarks," *IEEE Trans. on Image Processing*, vol. 25, no. 3, pp. 1047–1055, 2016.

[56] C. Lopez-Molina, B. De Baets, and H. Bustince, "Quantitative error measures for edge detection," *Pattern Recognition*, vol. 46, no. 4, pp. 1125–1139, 2013.

[57] F. J. Estrada and A. D. Jepson, "Benchmarking image segmentation algorithms," *International Journal of Computer Vision*, vol. 85, no. 2, pp. 167–181, 2009.

[58] P. Arbelaez, M. Maire, C. Fowlkes, and J. Malik, "Contour detection and hierarchical image segmentation," *IEEE Trans. on Pattern Analysis and Machine Intelligence*, vol. 33, pp. 898–916, 2011.

[59] C. Lopez-Molina, B. De Baets, H. Bustince, J. Sanz, and E. Barrenechea, "Multiscale edge detection based on Gaussian smoothing and edge tracking," *Knowledge-Based Systems*, vol. 44, pp. 101–111, 2013.